REPORT DOCUMENTATION PAGE

Form Approved
OMB NO. 0704-0188

1. AGENCY USE ONLY (Leave Blank)	2. REPORT DATE	3. REPORT TYPE AND DATES COVERED
	1 Sept 2004	Final Progress Report 1 Aug 01 - 31 July 04

4. TITLE AND SUBTITLE
COMPLETE DYNAMIC ROTOR WAKE MODEL IN STATE SPACE

5. FUNDING NUMBERS
~~GBUD #: 45667~~
~~Agreement #~~ DAAD19-01-1-0697

6. AUTHOR(S)
David A. Peters

7. PERFORMING ORGANIZATION NAME(S) AND ADDRESS(ES)
Washington University, Box 1185
St. Louis, Missouri 63130-4899

8. PERFORMING ORGANIZATION REPORT NUMBER
None

9. SPONSORING / MONITORING AGENCY NAME(S) AND ADDRESS(ES)
U. S. Army Research Office
P.O. Box 12211
Research Triangle Park, NC 27709-2211

10. SPONSORING / MONITORING AGENCY REPORT NUMBER
~~RPD~~
41304.11-EG

11. SUPPLEMENTARY NOTES
The views, opinions and/or findings contained in this report are those of the author(s) and should not be construed as an official Department of the Army position, policy or decision, unless so designated by other documentation.

12 a. DISTRIBUTION / AVAILABILITY STATEMENT
Approved for public release; distribution unlimited.

20040914 024

13. ABSTRACT (Maximum 200 words)

This research deals with the development of a finite-state inflow theory that will be able to predict all three components of flow both on and off of the rotor disk. The theory will be of a velocity potential expanded in hierarchical degrees of freedom.

14. SUBJECT TERMS	15. NUMBER OF PAGES
rotor wake model, induced flow, state space	23
	16. PRICE CODE

17. SECURITY CLASSIFICATION OR REPORT	18. SECURITY CLASSIFICATION ON THIS PAGE	19. SECURITY CLASSIFICATION OF ABSTRACT	20. LIMITATION OF ABSTRACT
UNCLASSIFIED	UNCLASSIFIED	UNCLASSIFIED	UL

A COMPLETE ROTOR WAKE MODEL IN STATE SPACE

David A. Peters

September 1, 2004

U.S. Army Research Office

Grant No. DAA19-01-1-0697

Washington University in St. Louis

FINAL PROGRESS REPORT

ARO Grant No. DAA19-01-1-0697

A Complete Rotor Wake Model in State Space
1 January 2003 through 31 December 2003

by

David A. Peters
Principal Investigator
McDonnell Douglas Professor of Engineering
Chairman, Department of Mechanical Engineering
Director, Center for Computational Mechanics
Associate Director, Georgia Tech/Washington University
Center of Excellence for Rotorcraft Technology
Washington University, Campus Box 1185
St. Louis, MO 63130

Objectives

The objective of this research is to develop a theory for the behavior of a rotor wake undergoing dynamic perturbations. The theory should be capable of finding the flow in all three directions both on the rotor disk and off of the rotor disk. The theory should be in a state-space form that is hierarchical and can be used in real-time simulation studies. It should include dynamic inflow and the He Dynamic Wake Model as special cases, and should be derived from first principles. It should allow for mass source terms as well as pressure differentials.

Approach

The approach taken is as follows:

1.) Formulate equations based on a Galerkin approach on the linearized potential flow equations for a rotor in a skewed free-stream.
2.) Develop all Galerkin integrals in closed form based on the divergence theorem.
3.) Study the convergence of the model for test cases with known solutions.
4.) Develop strategies to overcome singularities.

Accomplishments

The history of dynamic wake modeling covers the last 55 years. References [1] through [17] outline the work up to the 1990's. Several important developments followed that changed the course of dynamic wake modeling. First, there was an unusual anomaly in helicopter flight mechanics that, during a pitching maneuver, experimental flight-test data showed that rotorcraft rolled opposite to what the simulations predicted even with the new wake models. Rosen, Ref. [18], suggested that this might be due to the effect of wake curvature on induced flow during the maneuver.

Curtiss and coworkers investigated this and found that this curvature effect could explain part of the anomaly and that simple vortex and momentum considerations could

capture the effect, Refs. [19-20]. Barocela, corroborated these findings in his work on wake distortion, Ref. [21], although some discrepancies were noted with the work of Curtiss, Ref. [22]. Barocela showed that the effect of wake curvature could be incorporated into the dynamic wake model of Pitt and Peters by allowing the coefficient matrices to be functions of both the wake skew and the wake curvature. This was completed by Krothapalli, et. al in Ref. [23].

The work on wake curvature was extended to the He model in References [24-26] in which it was shown that the entire coefficient matrix (involving all harmonics) could be modified to account for wake curvature. Reference [27] demonstrated that the work of Curtiss could be considered a special case of this more general formulation, thus uniting all of the various formulations together.

Another area of work on dynamic wake came with the need for ground effect calculations. The original He theory had included a simple ground-effect correction, but it became clear that something more general was needed in order to accommodate moving ground planes, inclined ground planes, and partial ground planes. References [28-31] progressed through a series of developments in which the He inflow model was used to treat ground effect. In these various approaches, either an image rotor or a ground plane source rotor was used to simulate the ground in a quasi-steady manner. For these cases, a second actuator disk (for the image rotor or ground rotor) was used, and the induced flow from that rotor needed to be computed on the primary rotor. This was done numerically by an off-line quasi-steady approach.

From that work, it became clear that what was needed was a completely unsteady theory that could compute the induced flow of these secondary rotors above the disk plane and in all three components. The He model, however, was unable to do this; and, therefore, the need was established for a more general treatment of inflow dynamics. This led to an entirely new methodology for induced flow dynamics.

Reference [32] outlined an approach for deriving dynamic wake equations in terms of velocity potentials rather than merely normal velocity components at the rotor disk. Such a formulation was shown to be derivable from a Galerkin procedure applied to the potential flow equations. In Reference [33], this methodology was successfully implemented. Reference [34] demonstrated that this method contained the old He model (and, consequently, the Pitt-Peters model) as a special case in which off-disk modes were neglected. References [35-36] demonstrated that the method did, indeed converge for all three components of flow in the entire half space including the plane of the rotor disk and the semi-sphere above it.

Fluid-Dynamics Equations

The three-dimensional potential flow equations (momentum and continuity equations) for the pressure and velocity fields P and $\vec{v}$, with a free-stream velocity V_∞, are

$$\frac{\partial \vec{v}}{\partial \tau} - \frac{\partial \vec{v}}{\partial \xi} = -\vec{\nabla} P \qquad (1)$$

$$\vec{\nabla} \bullet \vec{v} = 0 \qquad (2)$$

These equations have been non-dimensionalized by defining P as pressure divided by ρV_∞^2, $\vec{v}$ as induced velocity divided by V_∞, and time as a reduced time τ, (i.e., time multiplied by V_∞/R.) The variable ξ is the non-dimensional coordinate along the free-stream line, positive upstream. All lengths are divided by the rotor radius R. Figure 1 shows the coordinate system.

From continuity, Eq. (2), it is observed that $\vec{v}$ can be expressed by a velocity potential that satisfies Laplace's equation. It can also be shown that P satisfies Laplace's equation. Therefore, P can be expressed as a summation of pressure potentials, Φ; and $\vec{v}$ can be expressed as a summation of the gradient of velocity potentials, Ψ.

Pressure Potentials, and Velocity Potentials

To transform Eqs. (1) and (2) by a Galerkin method, it is required to expand the pressure potential, Φ, and the velocity potentials, Ψ, in terms of a complete set of functions, each of which satisfies Laplace's equation. In addition, they have to fulfill the boundary conditions for pressure in the case of Φ, and for velocity in the case of Ψ.

The boundary conditions for pressure are given by a discontinuity across the rotor disk, Fig. (1). The use of an ellipsoidal coordinate system $[\nu,\eta,\overline{\psi}]$, has the advantage that any odd function in ν, will allow a representation of a discontinuity across the rotor disk. An additional advantage of using an ellipsoidal coordinate system is that an analytical solution of Laplace's equation is known and can be expressed as,

$$\Phi_n^{mc}(\nu,\eta,\overline{\psi}) = \overline{P}_n^m(\nu)\overline{Q}_n^m(i\eta)\cos(m\overline{\psi}) \qquad (3)$$

$$\Phi_n^{ms}(\nu,\eta,\overline{\psi}) = \overline{P}_n^m(\nu)\overline{Q}_n^m(i\eta)\sin(m\overline{\psi}) \qquad (4)$$

where $\overline{P}_n^m(\nu)$ and $\overline{Q}_n^m(i\eta)$ are normalized associated Legendre functions of first and second kind.

Since $\overline{P}_n^m(\nu)$ with $n+m$ odd is an odd function of ν as well as a function that satisfies Laplace's equation, it has a discontinuity across the disk. Therefore, Eqs. (3) and (4) can be used as the expansion functions for the pressure potentials. On the other hand, $\overline{P}_n^m(\nu)$ with $n+m$ even is an even function of ν, but its derivative with respect to z is an odd function of ν on the disk. Such functions can be used to represent mass sources at the rotor disk.

$$P = -\sum_{m=0}^{\infty}\sum_{n=m+1}^{\infty}\left(\tau_n^{mc}\Phi_n^{mc} + \tau_n^{ms}\Phi_n^{ms}\right) \qquad (5)$$

The boundary conditions for the velocity field are: (1) the velocity field far upstream from the rotor is equal to zero, and (2) there is a velocity discontinuity any place a vortex or vortex sheet exists in the flow field. These discontinuities only exist at the rotor blades and within the rotor wake.

If the velocity-field computational domain is limited to the infinite upper-half volume above the rotor disk (Fig.2) the functions to be used in the velocity expansion do not have to fulfill any discontinuity conditions. It is important to note that, in the case of perfectly edgewise flow, the wake is located on the rotor disk plane. Thus no convergence of this methodology is expected on the trailing region off the rotor disk for edgewise flow, since the assumption for the velocity potentials is no longer valid in this region.

In order to strongly satisfy the upstream boundary condition for the velocity field, the velocity potentials are defined as

$$\Psi_n^{mc} = \int_{\xi}^{\infty}\Phi_n^{mc}d\xi\,; \quad \Psi_n^{ms} = \int_{\xi}^{\infty}\Phi_n^{ms}d\xi$$

$$m = 0,1,2,\ldots,\infty; \quad n = m,m+1,m+2,\ldots,\infty \qquad (6)$$

This strongly ensures a zero velocity upstream. As ξ approaches infinity, Ψ_n^m approaches zero. The velocity $\vec{v}$ is taken as

$$\vec{v} = \sum_{m=0}^{\infty}\sum_{n=m}^{\infty}\left(\hat{a}_n^m\vec{\nabla}\Psi_n^{mc} + \hat{b}_n^m\vec{\nabla}\Psi_n^{ms}\right) \qquad (7)$$

where Ψ_n^{mc} and Ψ_n^{ms} are defined by Eq. (6).

Substitution of Eqs. (5) and (7) into (1), yields the momentum equation in an expansion form. Because $\hat{a}_n^m$, $\hat{b}_n^m$, τ_n^{mc} and τ_n^{ms} are functions of nondimensional time (τ); while Ψ_n^{mc}, Ψ_n^{ms}, Φ_n^{mc}, and Φ_n^{ms} are functions of the spatial coordinates (x, y, z), Eq. (1) takes the following form for cos ($\overline{\Psi}$) terms:

$$\sum_{m=0}^{\infty}\sum_{n=m}^{\infty}\left(\vec{\nabla}\Psi_n^{mc}\frac{d\hat{a}_n^m}{d\tau} - \vec{\nabla}\frac{\partial\Psi_n^{mc}}{\partial\xi}\hat{a}_n^m\right) = \sum_{m=0}^{\infty}\sum_{n=m+1}^{\infty}\vec{\nabla}\Phi_n^{mc}\tau_n^{mc} \qquad (8)$$

Only the cosine terms are listed, since sine and cosine completely decouple. However, an identical set of equations can be written for the sine terms.

Galerkin Approach

If a Galerkin approach is applied to solve the conservation of momentum equation, Eq.

(8) is pre-multiplied by the gradient of each one of some test functions, Λ, integrated over the domain; and the integrals are set to zero. In a Galerkin methodology, the test functions are defined from the same set of functions used to expand the pressure potential, Φ, and the velocity potentials, Ψ. Thus, we choose

$$\Lambda_j^{rc} = \Phi_j^{rc}; \qquad \Lambda_j^{rs} = \Phi_j^{rs}$$
$$r = 0,1,2,\ldots,\infty; \quad j = r, r+1, r+2, \ldots, \infty \tag{9}$$

When this Galerkin approach is applied, the conservation of momentum equation, Eq. (8), becomes

$$\iiint_V \vec{\nabla}\Lambda_j^{rc} \bullet \sum_{m=0}^{\infty}\sum_{n=m}^{\infty}\left(\vec{\nabla}\Psi_n^{mc}\frac{d\hat{a}_n^m}{d\tau} - \vec{\nabla}\frac{\partial\Psi_n^{mc}}{\partial\xi}\hat{a}_n^m\right)dV =$$
$$\iiint_V \vec{\nabla}\Lambda_j^{rc} \bullet \sum_{m=0}^{\infty}\sum_{n=m+1}^{\infty}\vec{\nabla}\Phi_n^{mc}\tau_n^{mc}\,dV$$
$$r = 0,1,2,\ldots,\infty; \quad j = r, r+1, r+2, \ldots, \infty \tag{10}$$

The Divergence Theorem allows volume integrals to be expressed as surface integrals, Fig. 2. Therefore, if this theorem is applied to Eq. (10), and because Λ_j^{rc}, Ψ_n^{mc}, and Φ_n^{mc} all fulfill Laplace's equation, Eq. (10) becomes

$$\sum_{m=0}^{\infty}\sum_{n=m}^{\infty}\iint_S\left(\Lambda_j^{rc}\frac{\partial\Psi_n^{mc}}{\partial\vec{n}}\frac{d\hat{a}_n^m}{d\tau} - \Lambda_j^{rc}\frac{\partial^2\Psi_n^{mc}}{\partial\vec{n}\partial\xi}\hat{a}_n^m\right)dS =$$
$$\sum_{m=0}^{\infty}\sum_{n=m+1}^{\infty}\iint_S\Lambda_j^{rc}\frac{\partial\Phi_n^{mc}}{\partial\vec{n}}dS\tau_n^{mc}$$
$$r = 0,1,2,\ldots,\infty; \quad j = r, r+1, r+2, \ldots, \infty \tag{11}$$

or

$$\sum_{m=0}^{\infty}\sum_{n=m}^{\infty}\iint_S\left(\frac{\partial\Lambda_j^{rc}}{\partial\vec{n}}\Psi_n^{mc}\frac{d\hat{a}_n^m}{d\tau} - \frac{\partial\Lambda_j^{rc}}{\partial\vec{n}}\frac{\partial\Psi_n^{mc}}{\partial\xi}\hat{a}_n^m\right)dS =$$
$$\sum_{m=0}^{\infty}\sum_{n=m+1}^{\infty}\iint_S\frac{\partial\Lambda_j^{rc}}{\partial\vec{n}}\Phi_n^{mc}dS\tau_n^{mc}$$
$$r = 0,1,2,\ldots,\infty; \quad j = r, r+1, r+2, \ldots, \infty \tag{12}$$

where S represents the surface area of the upper-half inflow volume V, including the rotor disk plane, dS represents a differential area element; and $\vec{n}$ is a unit-vector, outward normal to dS. The surface S can be subdivided into three areas: two of them are located on the rotor disk plane (z=0), s, and correspond to the on-disk area, A, and the off-disk area, B; and the third one corresponds to the area on the infinite dome, C (Fig.2). Therefore,

$$s = A + B; \quad S = s + C \tag{13}$$

The pressure potentials, Φ_n^{mc}, velocity potentials, Ψ_n^{mc}, and test functions, Λ_j^{rc}, are such that all the integrals over the dome surface, C, become zero. Therefore, the surface of integration becomes the rotor disk plane (z=0), s, and the normal outward vector is along the z axis. Therefore,

$$\frac{\partial}{\partial\vec{n}} = \frac{\partial}{\partial z} \tag{14}$$

If Eq. (14) is substituted into Eqs. (11) and (12), together with the definition of the velocity potentials and the test functions, Eqs. (6) and (9), they become

$$\sum_{m=0}^{\infty}\sum_{n=m}^{\infty}\iint_s\Phi_j^{rc}\left(\frac{\partial}{\partial z}\left(\int_0^{\infty}\Phi_n^{mc}d\xi\right)\frac{d\hat{a}_n^m}{d\tau} + \frac{\partial\Phi_n^{mc}}{\partial z}\hat{a}_n^m\right)ds =$$
$$\sum_{m=0}^{\infty}\sum_{n=m+1}^{\infty}\iint_s\Phi_j^{rc}\frac{\partial\Phi_n^{mc}}{\partial z}ds\tau_n^m$$
$$r = 0,1,2,\ldots,\infty; \quad j = r, r+1, r+2, \ldots, \infty \tag{15}$$

$$\sum_{m=0}^{\infty}\sum_{n=m}^{\infty}\iint_s\frac{\partial\Phi_j^{rc}}{\partial z}\left(\int_0^{\infty}\Phi_n^{mc}d\xi\frac{d\hat{a}_n^m}{d\tau} + \Phi_n^{mc}\hat{a}_n^m\right)ds =$$
$$\sum_{m=0}^{\infty}\sum_{n=m+1}^{\infty}\iint_s\frac{\partial\Phi_j^{rc}}{\partial z}\Phi_n^{mc}ds\tau_n^m$$
$$r = 0,1,2,\ldots,\infty; \quad j = r, r+1, r+2, \ldots, \infty \tag{16}$$

where ds is a differential area on z=0.

At this point, it is important to note that the Φ_n^m with $n+m$ odd are zero on the z=0 plane off the disk (B), whereas the z derivatives of Φ_n^m with $n+m$ even are zero on region B. Because of this, the Divergence theorem can be utilized with appropriate choice of the $\partial/\partial z$ position in each individual term such that all integrals are zero on region B. The result is a set of integrals that need only be evaluated on region A (on-disk) for which they can be evaluated in closed form. The expression obtained after applying this procedure can be condensed in the following equation.

$$\left[\tilde{L}^c\right]\left\{\hat{a}_n^m\right\}^* + \left[D^c\right]\left\{\hat{a}_n^m\right\} = \left[D^c\right]\left\{\tau_n^{mc}\right\} \tag{17}$$

where $(\,)^* = d(\,)/d\tau$ and where each one of the elements of the $\tilde{L}^c$ and D^c matrices are known in closed form.

Equation (17) is valid for any skew angle χ, which appears in the equation in the expressions for the wake influence coefficient matrix $\tilde{L}^c$. This equation can be further partitioned into two row-groups and two column-groups such that $m+n$ (or $j+r$) is odd and $m+n$ (or $j+r$) is even. These matrices are organized in the following way

$$\left[\begin{array}{c|c} \begin{bmatrix} j+r=odd, \\ n+m=odd \end{bmatrix} & \begin{bmatrix} j+r=odd, \\ n+m=even \end{bmatrix} \\ \hline \begin{bmatrix} j+r=even, \\ n+m=odd \end{bmatrix} & \begin{bmatrix} j+r=even, \\ n+m=even \end{bmatrix} \end{array}\right] \left\{\begin{array}{c} \{n+m=odd\} \\ \hline \{n+m=even\} \end{array}\right\} \tag{18}$$

If Eq. (17) is organized as suggested in Eq. (18), it can be partitioned as

$$\left[\begin{array}{c|c} [\tilde{L}]_{o,o} & [\tilde{L}]_{o,e} \\ \hline [\tilde{L}]_{e,o} & [\tilde{L}]_{e,e} \end{array}\right] \left\{\begin{array}{c} \{\hat{a}_n^{*m}\}_o \\ \hline \{\hat{a}_n^{*m}\}_e \end{array}\right\} + \left[\begin{array}{c|c} [D]_{o,o} & [D]_{o,e} \\ \hline [D]_{e,o} & [D]_{e,e} \end{array}\right] \left\{\begin{array}{c} \{\hat{a}_n^m\}_o \\ \hline \{\hat{a}_n^m\}_e \end{array}\right\} = \left[\begin{array}{c|c} [D]_{o,o} & [D]_{o,e} \\ \hline [D]_{e,o} & [D]_{e,e} \end{array}\right] \left\{\begin{array}{c} \{\tau_n^m\}_o \\ \hline \{\tau_n^m\}_e \end{array}\right\} \tag{19}$$

Potential Function Expansions

The non-dimensional pressure drop and mass flow added to the velocity field (both across the disk), and the velocity everywhere in the upper-half plane can be computed for the cosine terms as

$$\frac{\Delta p}{\rho V_\infty^2} = \left[P_{lower} - P_{upper}\right]_{\eta=0} = 2\sum_{m=0}^{\infty} \sum_{n=m+1,m+3,....}^{\infty} \bar{P}_n^m(\nu)\left(\tau_n^{mc}\right)_o \cos(m\bar{\psi}) \tag{20}$$

$$\frac{\Delta \dot{m}}{\rho V_\infty} = \left[P_{lower} + P_{upper}\right]_{\eta=0} = 2\sum_{m=0}^{\infty} \sum_{n=m+2,m+4,....}^{\infty} \bar{P}_n^m(\nu)\left(\tau_n^{mc}\right)_e \cos(m\bar{\psi}) \tag{21}$$

$$\vec{v} = \sum_{m=0}^{\infty}\sum_{n=m}^{\infty} \hat{a}_n^m \vec{\nabla} \Psi_n^{mc} = \sum_{m=0}^{\infty}\sum_{n=m}^{\infty} \hat{a}_n^m \vec{\nabla}\left(\int_\xi^\infty \Phi_n^{mc} d\xi\right) \tag{22}$$

From Eq. (22), it is seen that, to compute the velocity field, it is required to compute the velocity potentials, Ψ_n^m, by a numerical integration

$$\Psi_n^m = \int_\xi^\infty \Phi_n^{mc} d\xi \tag{23}$$

To avoid numerical integration and in order to be able to express the velocity potentials in terms of potentials known everywhere in the flow field, a change of variable from $\hat{a}_n^m$ to a_n^m is introduced

$$\left\{\hat{a}_n^m\right\}^T \left\{\Psi_n^{mc}\right\} = \left\{a_n^{mc}\right\}^T \left\{\sigma_n^m \Phi_{n+1}^{mc} + \varsigma_n^m \Phi_{n-1}^{mc}\right\} \tag{24}$$

The constants σ_n^m and ς_n^m are chosen such that the new velocity potentials will give no singularities when gradients are taken.

$$\sigma_n^m = \frac{1}{K_n^m \sqrt{(2n+1)(2n+3)\left((n+1)^2 - m^2\right)}} \tag{25}$$

$$\varsigma_n^m = \frac{1}{K_n^m \sqrt{\left(4n^2-1\right)\left(n^2-m^2\right)}}; n \neq m \tag{26}$$

where

$$K_n^m = \left(\pi/2\right)^{(-1)^{n+m}} H_n^m \tag{27}$$

$$H_n^m = \frac{(n+m-1)!!(n-m-1)!!}{(n+m)!!(n-m)!!} \tag{28}$$

and

$$\begin{aligned} &(n)!! = (n)(n-2)(n-4)...(2), n = even \\ &(n)!! = (n)(n-2)(n-4)...(1), n = odd \\ &(0)!! = 1;\ \ (-1)!! = 1;\ \ (-2)!! = \infty;\ \ (-3)!! = -1 \end{aligned} \tag{29}$$

If a Galerkin approach is applied to Eq. (24), the following relationship can be obtained

$$\left\{\hat{a}_n^m\right\} = \left[\tilde{L}^c\right]^{-1} \left[M^c\right] \left\{a_n^m\right\} \tag{30}$$

where

$$\left[M^c\right] = \left[\tilde{L}^c\right]_{\chi=0} \tag{31}$$

and where $\left[\tilde{L}^c\right]$ is the same matrix as defined in Eq. (17) and in the Appendix.

Equation (24) can be used to express the velocity potentials in axial flow. [32] If Eq. (24) is substituted into Eq. (22), it yields

$$v_z = \sum_{m=0}^{\infty}\sum_{n=m+1}^{\infty} a_n^m \vec{\nabla}\left(\sigma_n^m \Phi_{n+1}^{mc} + \varsigma_n^m \Phi_{n-1}^{mc}\right) \tag{32}$$

Since

$$\frac{\partial\left(\sigma_n^m \Phi_{n+1}^{mc} + \varsigma_n^m \Phi_{n-1}^{mc}\right)}{\partial z} = \Phi_n^m, n > m \tag{33}$$

the axial component of the velocity is given by

$$v_z = \sum_{m=0}^{\infty} \sum_{n=m+1}^{\infty} a_n^m \Phi_n^{mc} \qquad (34)$$

We recall that the He model came in two equivalent versions, one with velocities expressed in terms of $P_n^m(2)$, and one in terms of $\frac{1}{\nu} P_n^m(2)$. Thus, the Morillo model is similar to the first version of the He model but with both $m+n$ odd and $m+n$ even.

If Eq. (30) is substituted into Eq. (17), the set of ordinary differential equations for the velocity coefficients in terms of the pressure coefficients for skewed flow becomes,

$$\left[M^c\right]\left\{\dot{a}_n^m\right\}+\left[D^c\right]\left[\bar{L}^c\right]^{-1}\left[M^c\right]\left\{a_n^m\right\}=\left[D^c\right]\left\{\tau_n^{mc}\right\} \qquad (35)$$

In axial flow, this equation becomes,

$$\left[M^c\right]\left\{\dot{a}_n^m\right\}+\left[D^c\right]\left\{a_n^m\right\}=\left[D^c\right]\left\{\tau_n^{mc}\right\} \qquad (36)$$

Equation (35), if truncated to include only $m+n$ odd terms, is identical to the form of the He model in which velocities are expanded as $P_n^m(r)$. Therefore, the He model is implicitly included in this new model. Furthermore, since the Pitt model is a special case of the He model, the original Pitt-Peters is also part of Eq. (35).

RESULTS

In this section, we look at some of the results from the newest inflow methodology as compared with the older approach. We will consider results both in the frequency domain and in the time domain. In the frequency domain there are closed-form numerical expressions based on the convolution integral that can be used to compare the solutions with a known result. There are also closed-form solutions in the time domain to a step input. With these, we can determine the accuracy and convergence properties of the methods.

Figure 3 shows results in the plane of the rotor disk, through the y=0 center-line both on the disk (-1<x <+1) and up to one radial length off the disk (-2<x<+2). The normal component of flow is plotted for an elliptical pressure distribution at zero frequency. The wake skew angle is zero, corresponding to purely axial flow as in hover or climb. The "exact" convolution result is compared with both the newer Galerkin approach and the older He model. For this case, all three results are identical. Only the real portion is present because of the zero frequency. Figure 4 shows the same results but at a reduced frequency of 2.3. Here, the new approach and the convolution have identical real and imaginary parts, but the older He model shows some error (of the order of 10%). This is the worst case for discrepancy between the old and new models. The difference is due to the coupling with off-disk inflow modes that are neglected in the He approach.

Figure 5 shows the same result, but for a cyclic pressure input and at a wake sew angle of 45° and zero frequency. Once again, the convolution approach, the He model, and the new model are identical. Figure 6 takes the same case but adds a reduced frequency of 4.0. Some error begins to show up in the new model downstream since convergence is slower for that case, and only ten shape functions are included in these results. The He method gives results only on the disk (not off); but it, too starts to deteriorate in accuracy toward the rear of the disk.

Figure 7 gives a more detailed examination of convergence with number of even terms added to the old He model. The graph gives an error norm (based on the square of velocity errors either on the rotor disk, -1<x<+1, or off-disk, -2<x<+2) for the normal component of velocity in axial flow. Ten terms are included in the old He shape functions ($n+m$ odd), and the number of new terms ($n+m$ even) is varied from zero to twelve. (Note, since terms come in alternating values of odd or even subscripts, there are half as many odd or even terms as the value of the highest subscript.) One can see how the error quickly converges to zero both on disk and off disk. However, if too many even terms or added, numerical ill-conditioning can cause the error to climb back up. Therefore, an optimum approach is to take only 3/4 as many even terms as there are odd terms.

Figure 8 demonstrates convergence for flow off the disk. The skew angle is a

relatively steep 75°. Flow is plotted one rotor radius above the disk along the disk centerline both on and off of the disk. The normal component of velocity is computed for 10 odd and 10 even terms and also for the optimized 10 odd and only 7 even terms. One can see that there is improved convergence when fewer $m+n$ even terms are included than there are $m+n$ odd terms. The reason for this is that, while the $m+n$ odd terms (the old He theory) are very-well conditioned, the $m+n$ even terms are poorly conditioned. Thus, round-off errors build more rapidly in these new terms. Fortunately, the on-disk terms give a good on-disk result, so that only a few off-disk are needed. Then flow both on the disk and off the disk is satisfactory.

Similar results are obtained for the other two velocity components (azimuthal and radial), as shown in Fig. 9, which gives all three components of flow for a cyclic input at zero degrees skew angle. Peters-He results are only shown for the z component since that is the only component for which the model can produce results.

In addition to the above frequency domain results, correlations have also been done in the time domain. Figures 10 and 11 show results in the time domain for a step input in pressure. The normal component of flow is plotted for the case of axial flow and for a reduced time up to $\tau=7$. The exact solution is compared to the finite-state results with 10 even and 10 odd terms. Flow is plotted at the disk center, one-half radius out from the center and one radius out from the center. Virtually exact agreement is obtained. Figure 10 compares this result with that of the old Peters-He model at the rotor center and at the rotor edge. The Peters-He model does very well for this case.

Non-Zero Mass Flux

The next step is to try to include terms with a non-zero net mass flux along any blade, Φ_n^m. This is based on the fact that these terms yield infinite kinetic energy in the flow field. Without losing generality, assume a pressure distribution $P=-\Phi_0^0$. The vertical component of induced velocity yields

$$v_z=\Phi_0^0=\bar{P}_0^0(\nu)\bar{Q}_0^0(i\eta) \tag{37}$$

and therefore

$$v_z=\begin{cases}\bar{P}_0^0(\nu)=1 & \text{on-disc}\\ \bar{Q}_0^0(i\eta)=\dfrac{2}{\pi}\tan^{-1}\left(\dfrac{1}{\eta}\right) & \text{off-disc}\end{cases} \tag{38}$$

For off-disc area, if Taylor series is used for large η

$$v_z=\frac{2}{\pi}\tan^{-1}\left(\frac{1}{\eta}\right)=\frac{2}{\pi}\left(\frac{1}{\eta}-\frac{1}{3\eta^3}+\cdots\right) \tag{39}$$

then the kinetic energy per unit mass of the induced flow crossing the off-disc rotor plane ($\nu=0$, $a\le\eta<\infty$) is that

$$T=\frac{1}{2}\iint_s v_z^2\,ds=\frac{4}{\pi}\int_a^\infty\left(\frac{1}{\eta}-\frac{1}{3\eta^3}\right)^2\eta\,d\eta=\infty \tag{40}$$

Equation (40) fully expresses the major discrepancy of including non-zero net mass flux terms in the model: Involvement of net mass flux terms, which happens in tremendous practical cases, will theoretically introduce infinite energy in the flow field. However, we know that mass source rotors exist in reality, and that they do not have infinite kinetic energy. This is due to two facts: the media field of the theory does not dissipate energy at all, and the whole system, including the media field to a distance of infinity, is in steady state. In reality, first of all, damping of air, even though very small under the condition of helicopter operating, will actually dissipate the energy and the induced velocity decreases much faster away from the rotor than those shown in Eq. (39). And secondly, the operating period of helicopter is not infinite. Furthermore, the study of induced flow is not the final goal in the study of helicopter's performance – the ultimate goal is to see how it affects the behavior of helicopter blades, fuselage or personnel on the ground if it is close to the

ground. Therefore, the most important concern is the area on or close to the actuator disc. Based on this aspect, if the results have good correlation at on-disc, or close-to-disc, area, the involvement of net mass flux could be tolerated.

On the other hand, the resultant infinities in $[\mathbf{M}^c]$ and the influence coefficient matrix $[\tilde{\mathbf{L}}^c]$ have no effect on the damping matrix $[\mathbf{D}^c]$, which is the coefficient matrix of the pressure coefficient vector on the right hand side. Therefore, it might be possible to include $m=n$ in τ_n^m but not in the velocity potentials.

To include net mass flux terms, i.e., $\bar{P}_m^m(\nu)$ and $\bar{Q}_m^m(i\eta)$, in the pressure distribution, the damping coefficient matrix $[\mathbf{D}^c]$ on the right hand side will be required to have extra columns. Based on the goal that the new model should reduce to Eq. (17) if net mass flux terms are not considered, these new entrees are desired to follow the same formulation of $[\mathbf{D}^c]$. Thus, we use the same formulas as in the Appendix but with $m=n$ allowed on the right-hand side.

Considering that the matrices on the left hand side have to be square, the extended momentum equation is expressed as

$$[\mathbf{M}^c]\{\dot{a}_n^m\}+[\mathbf{D}^c][\tilde{\mathbf{L}}^c]^{-1}[\mathbf{M}^c]\{a_n^m\}=[\bar{\mathbf{D}}^c]\{\tau_n^{mc}\} \quad (41)$$

where $[\bar{\mathbf{D}}^c]$ is the extended damping matrix.

Results with Mass Flux

Figures 12–16 illustrate the on-disc optimized frequency responses of pressure distribution $P=-\Phi_0^0$ with various system configurations. In all plots, circles are results from the convolution integral; triangles are results from closed-form solutions, which are available in limited cases; and dots represent results of the proposed state-space model by Galerkin approach.

As discussed, the velocity expansion excludes any terms with $m=n$, in which $m=n=0$ is an extreme case. Notice if the pressure distribution is $P=-\Phi_0^0$, From Eq. (16), the closed-form solution of the z-component of on-disc velocity perturbation is uniform. However, there is no function in the velocity expansion that has property of uniformity on-disc. In a general sense, it requires a large number of terms in the velocity expansion to yield a good approximation. On the off-disc area, the Galerkin approach decays into the far field faster than the exact solution. This is expected since we have no $1/\eta$ terms in the velocity expansions.

Figure 13 is the frequency response for infinite frequency. Based on the fact that the response actually becomes zero in such cases, ωv_i, $i=z,r,\bar{\psi}$, is plotted instead of ν. It shows that the on-disc and far off-disc areas have good correlation with the exact solution, yet relatively large oscillations appear at the edge of actuator. This is a consequence of using continuous expansion functions approximate a continuous velocity expansion.

Based on individual error analyses, optimized results of frequency response under various conditions are obtained and plotted in Fig. 14.

Figure 14 shows response of a higher frequency, skewed-angle flight. Fig. 14 shows good correlations in all four non-zero components. This is a direct result of increase of excitation frequency.

For purposes of illustration of generality of the model, Figs. 15 and 16 are presented to show the responses of pressure distribution $P=-\Phi_1^1$ with zero and infinite frequencies.

From all the plots, it can be seen that the radial components always have good correlation with the exact solution, even when the axial components yields large error. In cases of on-disc optimization, the low power radial function will decrease off-disc errors and therefore yields better correlations.

Thus, the theory with the extended [D] matrix allows for non-zero net mass flow.

Effect of Wake Curvature

The Pitt-Peters and Peters-He models involve the wake skew angle in the equations of motion. The skew angle appears in the form of

X = tan(χ/2) where χ is the skew angle. Interestingly, in the coupling between the m-th and r-th harmonic, X appears only to the powers (m+r) and (m-r). It is envisioned that the wake curvature angle will appear in a similar way. However, since the wake curvature is small, only terms to the first power in κ are used. These have been determined to involve only the cross-coupling between the zeroeth and first harmonics, and this has been done for the He model but not, as yet, for the newer Morillo model.

Figures

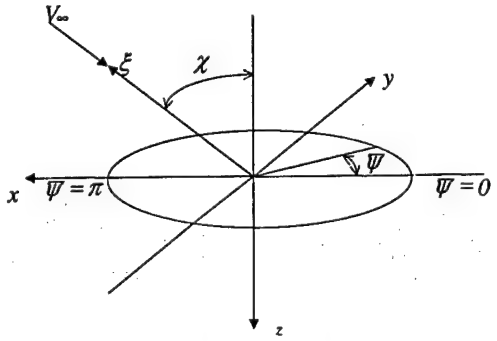

Fig.1 Coordinate system.

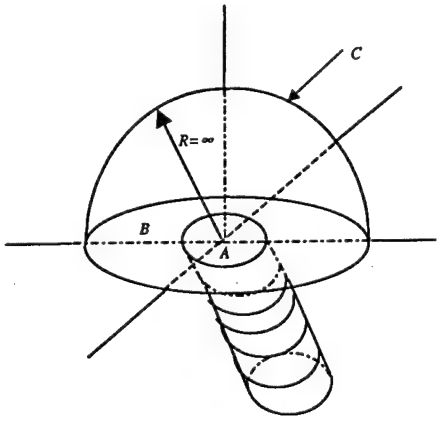

Fig.2 Volume and area of integration.

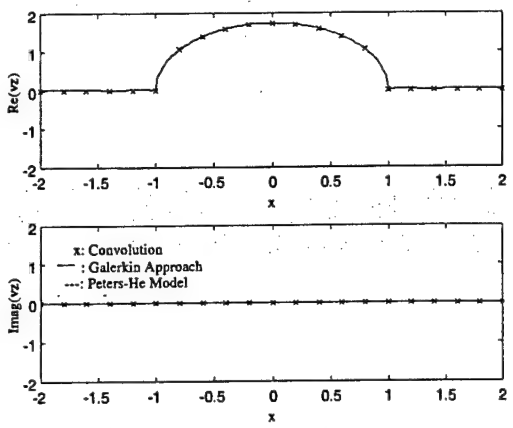

Fig. 3 Zero frequency response, $P=\Phi_1^0$, $\chi=0^o$.

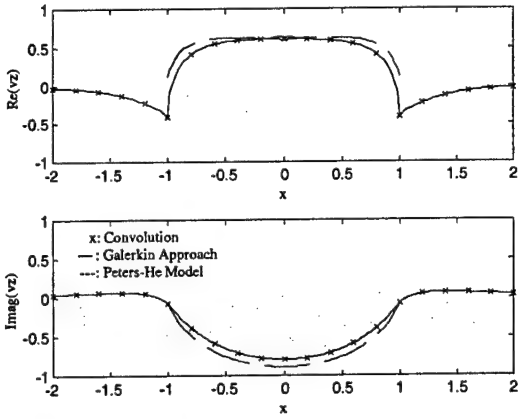

Fig. 4 Frequency response $\omega=2.3$, $P=\Phi_1^0$, $\chi=0^o$.

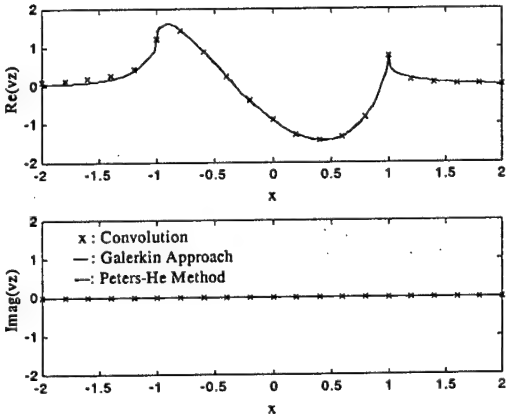

Fig. 5 Zero frequency response, $P=\Phi_2^1$, $\chi=45^o$.

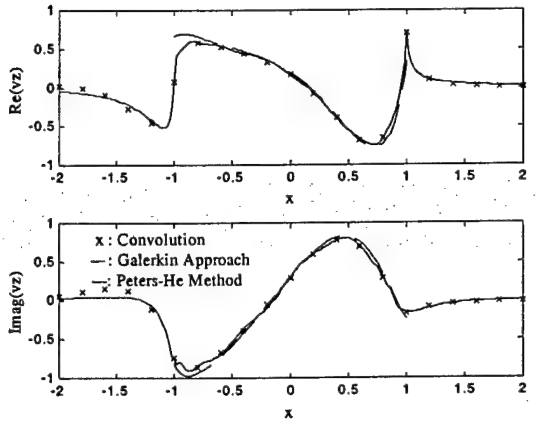

Fig. 6 Frequency response, ω=4, $P = \Phi_2^1$, χ=45°.

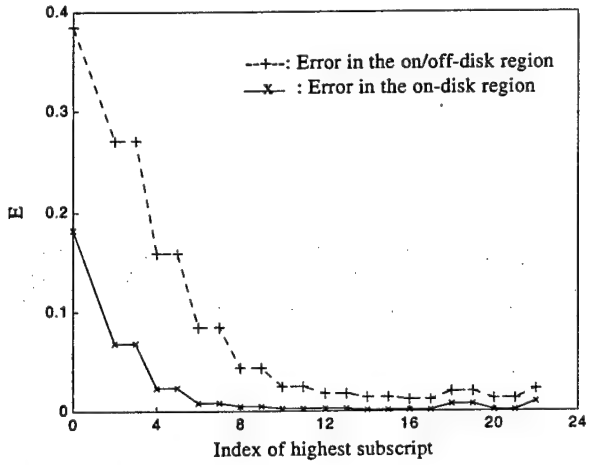

Fig. 7 Error, ω=2.3, $P = \Phi_1^0$, χ=0°, m_{odd}=20.

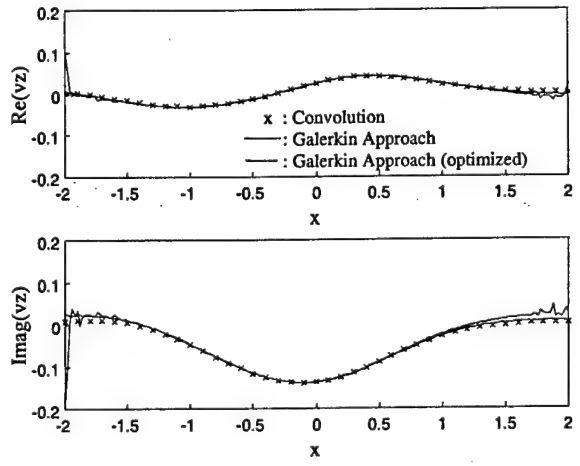

Fig. 8 Frequency response, ω=4.0, $P = \Phi_1^0$, χ=75°, z=-1.

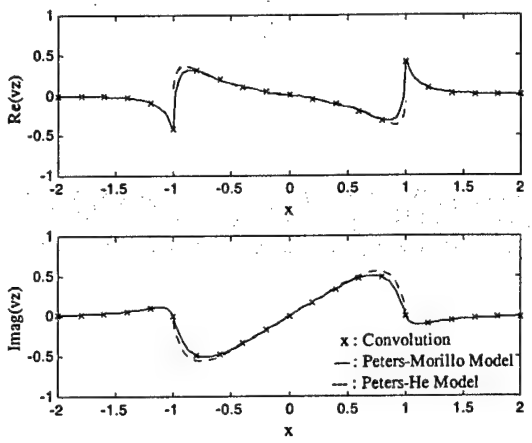

(a)

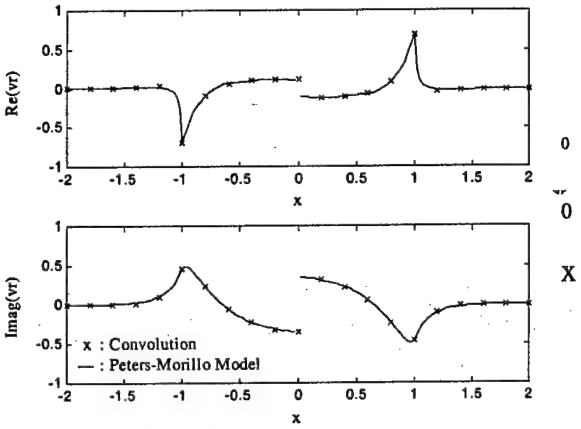

(b)

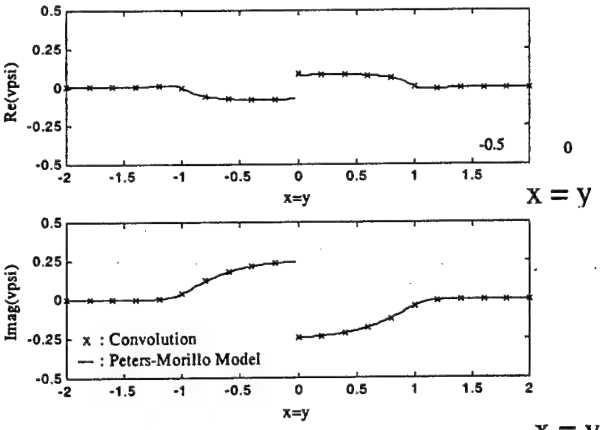

(c)

Fig. 9 Frequency response ω=7.3, $P = \Phi_2^1$, χ=0°.

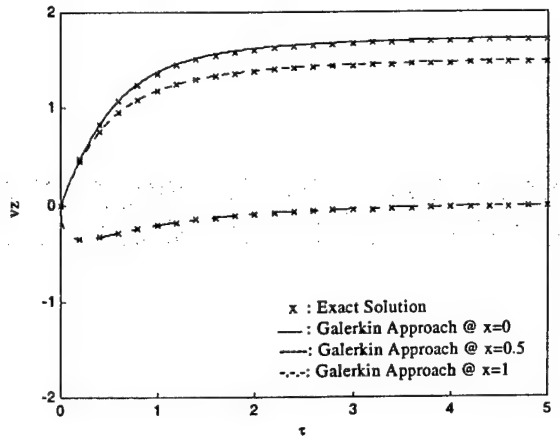

Fig. 10 Time response, $P = \Phi_1^0$, $\chi=0^o$, $z=0,y=0$.

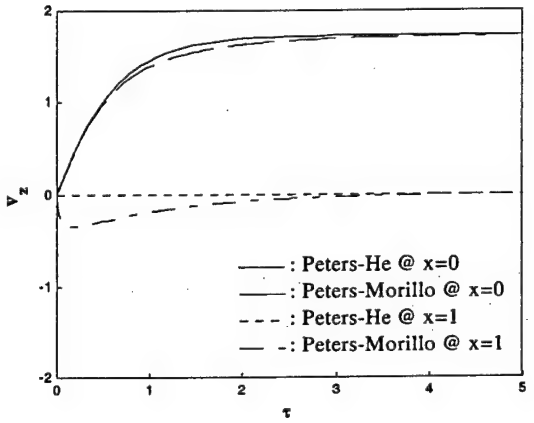

Fig. 11 Time response, $P = \Phi_1^0$, $\chi=0^o$, $z=0,y=0$.

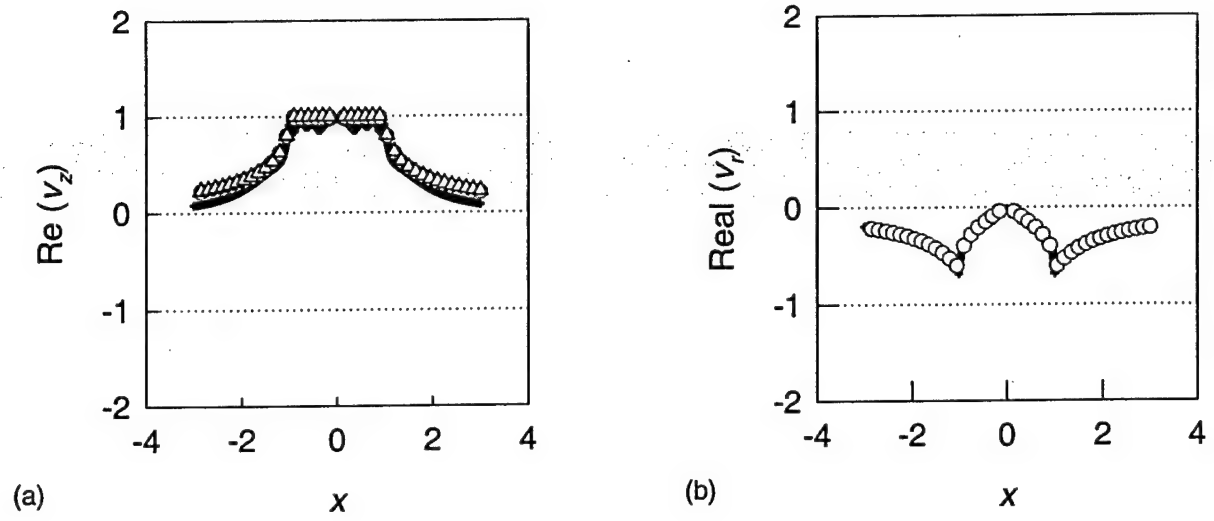

Figure 12. Frequency response of pressure distribution $P=-\Phi_0^0$ with $\omega=0$. All other components of induced velocities are zeroes. Both number of odd and even terms included in state-space model are 11. Highest power of radial polynomials is 22. Responses are evaluated with $z=0^-$ (on the actuator plane), $\chi=0$ (axial inflow), $\bar{\psi}=0^\circ,180^\circ$ (along fore-and-aft axis). Red circles present values of convolution integral results at locations; blue triangles present results of closed-form solution; and black dots present results obtained by Galerkin approach.

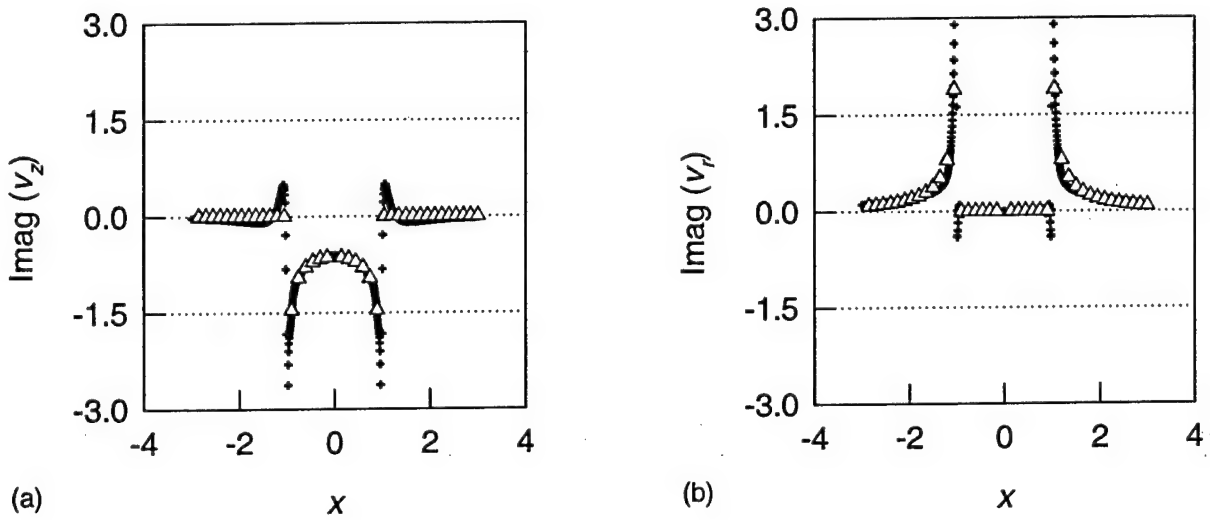

Figure 13. Frequency responses of pressure distribution $P=-\Phi_0^0$ with $\omega=\infty$. All other components of induced velocities are zeroes. Number of odd terms included in the state-space model is 10; Number of even terms is 3. Highest power of radial polynomials is 20. Responses are evaluated with $z=0^-$ (on the actuator plane), $\chi=0$ (axial inflow), $\bar{\psi}=0^\circ,180^\circ$ (along fore-and-aft axis). Blue triangles present results of closed-form solution; and black dots present results obtained by Galerkin approach.

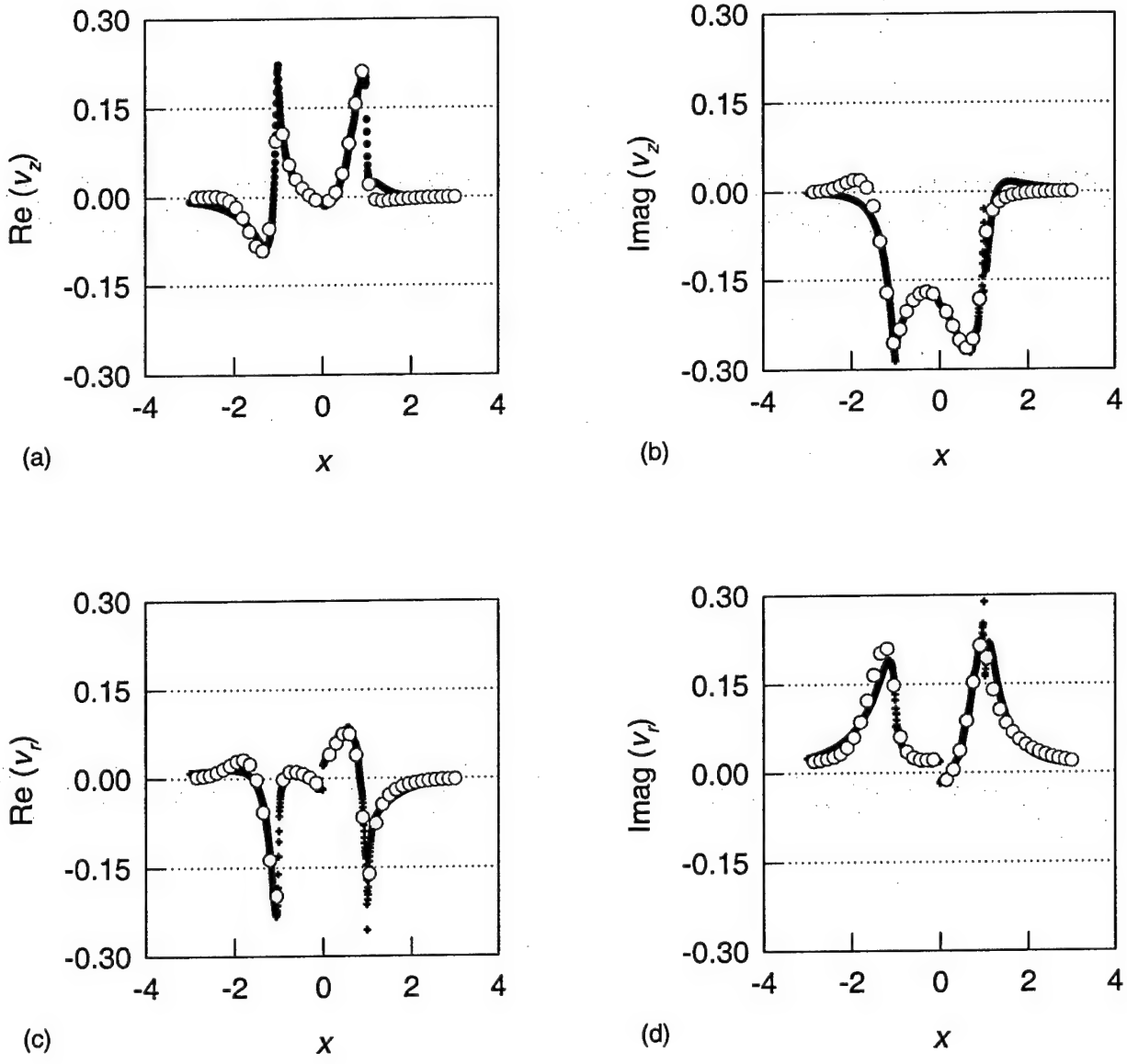

Figure 14. Frequency responses of pressure distribution $P=-\Phi_0^0$ with skew angle $\chi=45^\circ$, frequency $\omega=4$. Number of odd terms is 12; number of even terms is 4. Highest power of radial polynomials is $N_r=24$. Evaluation is performed on the actuator plane, $z=0^-$. Plots (a) and (b) are real and imaginary parts, respectively, of vertical component of induced velocity. Plots (c) and (d) are those of radial component of induced velocity. Red circles present values of convolution integral results at locations; and black dots present results obtained by Galerkin approach.

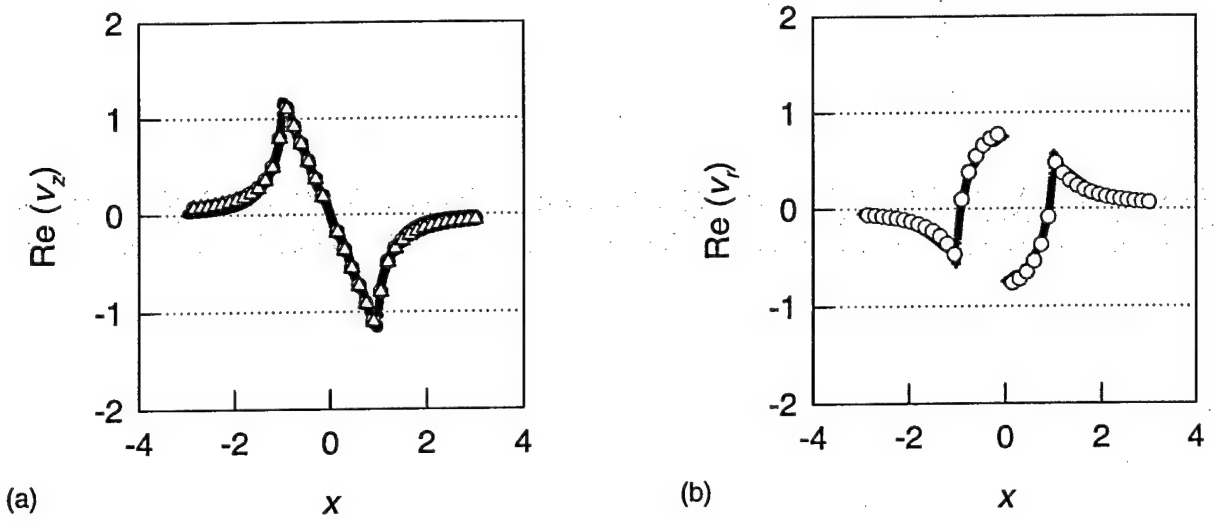

Figure 15. Frequency response of pressure distribution $P=-\Phi_1^1$ with $\omega=0$. All other components of induced velocities are zeroes. Numbers of odd and even terms included in state-space model are 11 and 10, respectively. Highest power of radial polynomial is 21. Responses are evaluated with $z=0^-$ (on the actuator plane), $\chi=0$ (axial inflow), $\bar{\psi}=0^\circ,180^\circ$ (along fore-and-aft axis). Red circles present values of convolution integral results at locations; blue triangles present results of closed-form solution; and black dots present results obtained by Galerkin approach.

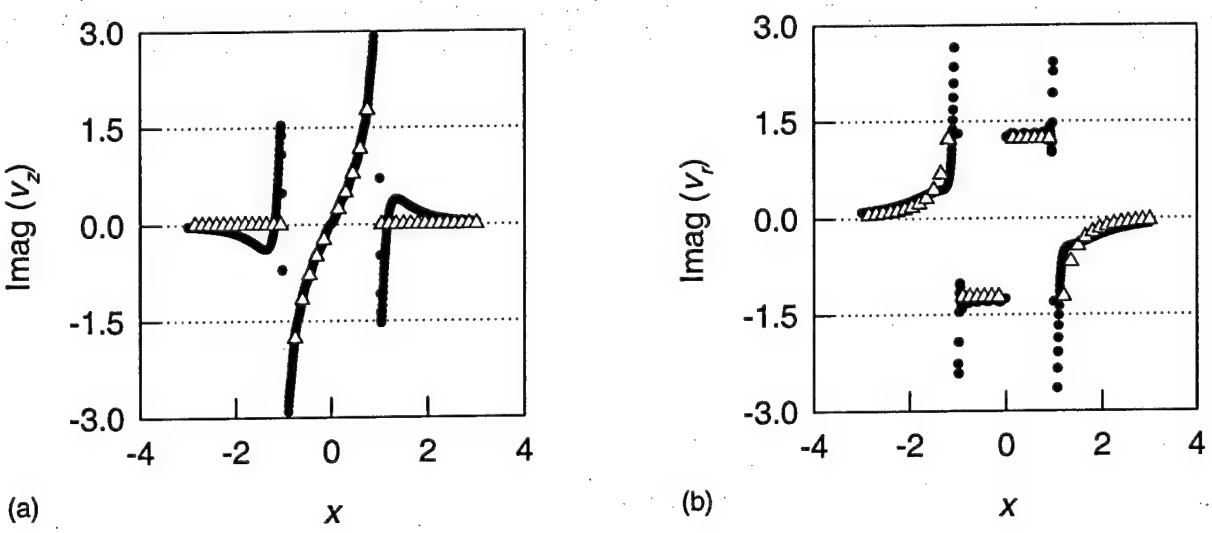

Figure 16. Frequency response of pressure distribution $P=-\Phi_1^1$ with $\omega=\infty$. All other components of induced velocities are zeroes. Numbers of odd and even terms included in state-space model are 12 and 4, respectively. Highest power of radial polynomial is 23. Responses are evaluated with $z=0^-$ (on the actuator plane), $\chi=0$ (axial inflow), $\bar{\psi}=0^\circ,180^\circ$ (along fore-and-aft axis). Red circles present values of convolution integral results at locations; blue triangles present results of closed-form solution; and black dots present results obtained by Galerkin approach.

REFERENCES

1. Amer, Kenneth B., "Theory of Helicopter Damping in Pitch or Roll and Comparison with Flight Measurements," NASA TN 2136, October 1948.
2. Sissingh, G.J., "The Effect of Induced Velocity Variation on Helicopter Rotor Damping in Pitch or Roll," A.R.C. Technical Report G.P. No. 101 (14,757, 1952.
3. Carpenter, P.J. and Fridovich, B., "Effect of a Rapid Blade Pitch Increase on the Thrust and Induced Velocity Response of a Full Scale Helicopter Rotor," NASA TN 3044, Nov., 1953.
4. Loewy, Robert G., "A Two Dimensional Approach to the Unsteady Aerodynamics of Rotary Wings," *Journal of the Aerospace Sciences,* Vol. 24, 1957, pp. 82-98.
5. Jones, J.P., "An Actuator Disc Theory for the Shed Wake at Low Tip Speed Ratios," MIT Aeroelasticity and Structures Laboratory Technical Report 133-1, 1965.
6. Joglekar, M. and Loewy, R., "An Actuator-Disc Analysis of Helicopter Wake Geometry and the Corresponding Blade Response," USAAVLABS, Technical Report 69-66, 1970.
7. Curtiss, Howard C., Jr., and Shupe, Norman K., "A Stability and Control Theory for Hingeless Rotors," Annual National Forum of the American Helicopter Society, Washington, D.C., May 1971.
8. Ormiston, R.A., and Peters, D.A., "Hingeless Helicopter Rotor Response with Non-Uniform Inflow and Elastic Blade Bending," *Journal of Aircraft*, Vol. 9, No. 10, Oct. 1972, pp 34-39.
9. Peters, D.A., "Hingeless Rotor Frequency Response with Unsteady Inflow," AHS/NASA Ames Specialists' Meeting on Rotorcraft Dynamics, NASA SP-362, February 1974.
10. Pitt, Dale Marvin, *Rotor Dynamic Inflow Derivatives and Time Constants from Various Inflow Models,* Doctor of Science Thesis, Washington University, December 1980.
11. Pitt, Dale M. and Peters, David A., "Theoretical Prediction of Dynamic-Inflow Derivatives," *Vertica*, Vol. 5, 1981, pp. 21-34.
12. Pitt, Dale M. and Peters, David A., "Rotor Dynamic Inflow Derivatives and Time Constants from Various Inflow Models," Ninth European Rotorcraft Forum, Stresa, Italy, September 13-15, 1983, Paper No. 55.
13. Peters, David A., Boyd, David Doug, and He, Cheng Jian, "A Finite-State Induce-Flow Model for Rotors in Hover and Forward Flight," *Journal of the American Helicopter Society,* Vol. 34, No. 4, October 1989, pp. 5-17.
14. Peters, David A. and He, C-J, "Correlation of Measured Induced Velocities with a Finite-State Wake Model," *Journal of the American Helicopter Society,* Vol. 36, No. 3, July 1991, pp. 59-70.
15. Su, Ay, Yoo, Kyung M., and Peters, David A., "Extension and Validation of an Unsteady Wake Model for Rotors," *Journal of Aircraft,* Vol. 29, No. 3, May-June, 1992, pp. 374-383.
16. Peters David A. and Su, Ay, "An Integrated Airloads-Inflow Model for Use in Rotor Aeroelasticity and Control Analysis," 47 Annual Forum of the American Helicopter Society, Phoenix, May 6-8, 1991.
17. Peters, David A. and Cao, Wenming, "Off-Rotor Induced Flow by a Finite-State Model," 37 AIAA SDM Conference, Salt Lake City, April 15-17, 1996, Paper 96-1550.
18. Rosen, A. and Isser A., "A New Model of Rotor Dynamics During Pitch and Roll of a Helicopter," *Journal of the American Helicopter Society*, Vol. 40, (3), July, 1995.
19. Keller, J.D. and Curtiss, H.C., Jr., "Modelling the Induced Velocity of a Maneuvering Helicopter," Proceedings of the American Helicopter Society 52nd Annual Forum, Washington, D.C., June 4-6, 1996, pp 841-851.
20. Keller, J.D., "An Investigation of Helicopter Dynamic Coupling Using an Analytical Model," *Journal of the American Helicopter Society*. Vol. 41, (3), July 1995.

21. Barocela, E., Peters, D.A., Krothapaiil, K.R. and Prasad, J.V.R., "The Effect of Wake Distortion on Rotor Inflow Gradients and Off-Axis Coupling," AIAA paper 97-3559, 1997.
22. Curtiss, H.C. Jr., "Aerodynamic Models and the Off-Axis Response," Proceedings of the American Helicopter Society 55th Annual Forum, Montreal, Canada, May 25-27, 1999.
23. Krothapalli, K.R., Prasad, J.V.R., Peters, D.A., "Helicopter Rotor Dynamic Inflow Modeling for Maneuvering Flight," Proceedings of the 55th Annual National Forum of the AHS, The Society for Vertical Flight, Montreal, May 14-17, 1999, pp. 498-510.
24. Prasad, J.V.R., Zhao, J. and Peters, D.A., "Modeling of Rotor Dynamic Wake Distortion During Maneuvering Flight," Proceedings of the 2001 AIAA Atmosphere Flight Mechanics Conference, Montreal, Canada, 2002.
25. Zhao, J., Prasad, J.V.R. and Peters, D.A., "Rotor Dynamic Wake Distortion Model for Helicopter Maneuvering Flight." Presented at the 58th Annual Forum of the American Helicopter Society, Montreal, Canada, 2002.
26. Zhao, J., Prasad, J.V.R. and Peters, D.A., "Simplified Dynamic Wake Distortion Model for Helicopter Transitional Flight." presented at the AIAA Atmospheric Flight Mechanics Conference, Monterey, AIAA-2002-4400.
27. Prasad, J.V.R., Zhao, Jinggen, and Peters, David A. "Helicopter Rotor Wake Distortion Models for Maneuvering Flight," Proceedings of the 28th European Rotorcraft Forum, Bristol, UK, September 17-20, 2002, Pages 17.1-17.9.
28. Prasad, J. V. R., Xin, Hong, Peters, D. A., Nagashima, T. and Iboshi, N., "Development and Validation of a Finite State In-Ground Effect Inflow Model for Lifting Rotors," Proceedings of the AHS Technical Specialists' Meeting for Rotorcraft Acoustics and Aerodynamics, Stratford, Connecticut, October 28-30, 1997.
29. Xin, et al, "Ground Effect Aerodynamics of Lifting Rotors Hovering above Inclined Ground Plane," presented at the AIAA Applied Aerodynamics and CFD Conference, Norfolk, Virginia, June 28 – July 1, 1999, AIAA-99-3223.
30. Xin, Hong, Prasad, J. V. R., Peters, D. A., "Dynamic Inflow Modeling for Simulation of a Helicopter Operating in Ground Effect," presented at the AIAA Modeling and Simulation Technology Conference, Portland, Oregon, August 9 – 11, 1999, AIAA-99-4114.
31. Xin, H., Prasad, J. V. R., Peters, D., Ibushi, N. and Nagashima, T., "Correlation of Experimental Measurements with a Finite-State Ground Effect Model," Proceedings of the 56th Annual National Forum of the American Helicopter Society, Virginia Beach, May 1-4, 2000, pp. 421–430.
32. Peters, David A. and Morillo, Jorge A., "Towards a Complete Dynamic Wake Model in Axial Flow," Proceedings of the American Helicopter Society Aeromechanics Specialists' Meeting, Atlanta, Georgia, November 13–14, 2000.
33. Morillo, Jorge A. and Peters David A., "Extension of Dynamic Inflow Models to Include Mass Injection and Off-Disk Flow," Proceedings of the 40th AIAA Aerospace Sciences Meeting & Exhibit, Paper No. AIAA-2002-0716. Reno, Nevada, January 14-17, 2002.
34. Morillo, Jorge A., *A Fully Three-Dimensional Unsteady Rotor Inflow Model from a Galerkin Approach,* Doctor of Science Dissertation, Washington University, December 2001.
35. Morillo, Jorge A. and Peters, David A., "Convergence of a Complete Finite State Inflow Model of a Rotor Flow Field," Proceedings of the 28th European Rotorcraft Forum, Bristol, UK, September 17-20, 2002, Pages 66.1-66.10.
36. Morillo, Jorge A. and Peters, David A., "Velocity Field Above a Rotor Disk by a New Dynamic Inflow Model," *Journal of*

Aircraft, Vol. 39, No. 3, September-October 2002.

37. Zhao, J., Prasad, J.V.R., Peters, D.A., "Investigation of Wake curvature Dynamics for Helicopter Maneuvering Flight Simulation," Proceedings of the AHS International 59th Annual Forum, Phoenix, May 6-8, 2003, pp. 1887-1901.

Appendix I

FORMS OF EXACT SOLUTIONS

$$\frac{\partial v}{\partial t}+\frac{\partial v}{\partial z}=-\frac{\partial P}{\partial z} \qquad v(z,0)=v_0(z)$$

$$P(z,t)=f(t)P(z) \qquad t\geq 0$$
$$P(z,t)=0 \qquad t<0$$

Homogenous: $v(x,t)=v_0(z-t)$

Step Input:

Outside wake: $v_{OW}(z,t)=P(z-t)-P(z)$

Inside wake: $v_{IW}(z,t)=2P_0+P(z-t)-P(z)$

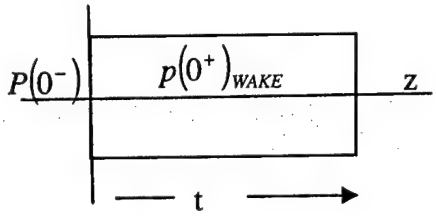

General Solutions: $P(0^+)\equiv P_0 \qquad f(0^+)\equiv f_0$

$$v_{OW}=f_0[P(z-t)-P(z)]+\int_{0^+}^{t}\dot{f}(\tau)[P(z-t+\tau)-P(z)]d\tau$$

$$v_{IW}=v_{OW}+2f_0P_0+2P_0\int_{0^+}^{t-z}\dot{f}(\tau)d\tau \qquad 0<z<t$$

Add Closed-Form Integrals:

$$v_{OW}=f_0P(z-t)-f(t)P(z)+\int_{0^+}^{t}\dot{f}(\tau)P(z-t+\tau)d\tau$$

$$v_{IW}=v_{OW}+2P_0\,f(t-z) \qquad 0<z<t$$

Move dot from f to P

$$v_{OW} = -\int_{0^+}^{t} \dot{f}(\tau) P(z-t+\tau)\, d\tau$$

$$v_{IW} = v_{OW} + 2P(0^+) f(t-z) \qquad 0 < z < t$$

$$v_{IW} = -\barint_0^t f(\tau)\, P_z(z-t+\tau)\, d\tau + \left[P(0^+) - P(0^-)\right] f(t-z)$$

Note: $IW \,//\, \int_0^t f(\tau)\, P_z(z-t+\tau)\, d\tau = f(t-z) \quad \left[P(0^+) - P(0^-)\right] f(t-z) + \barint_0^t f(\tau) P_z(z-t+\tau)\, d\tau$

Note: $\barint_0^t \equiv \lim_{\varepsilon \to 0} \int_0^{t-z-\varepsilon} + \int_{t-z+\varepsilon}^{t}$

Change to $\xi = z - t + \tau$

$$v_{OW} = -\int_{z-t}^{z} f(\xi - z + t) P_z(\xi)\, d\xi$$

$$v_{IW} = -\int_{z-t}^{z} f(\xi - z + t)\, P_z(\xi)\, d\xi + f(t-z)\left[2P(0^+)\right]$$

$$= \underbrace{-\int_{z-t}^{z} f(\xi - z + t) P_z(\xi)\, d\xi}_{\text{continuous}} + \underbrace{f(t-z) \quad \left[P(0^-) + P(0^+)\right]}_{\text{added mass flow}}$$

$$\vec{v}_{OW} = -\int_{z-t}^{z} f(\xi - z + t) \vec{\nabla} P(\xi)\, d\xi$$

since $f(\theta) = 0 \qquad \theta < 0$

$$\boxed{\vec{v} = -\barint_{-\infty}^{z} f(\xi - z + t) \vec{\nabla} P(\xi)\, d\xi + f(t-z)\underbrace{\left[P(0^+) + P(0^-)\right]}_{\text{in wake}}}$$

Exact Solution Skewed

Outside wake

$$\vec{v} = -\int_{-\infty}^{\xi} f(\eta - \xi + t) \vec{\nabla} P(\eta)\, d\eta$$

Check

$$\frac{\partial \vec{v}}{\partial t} = -\int_{-\infty}^{\xi} f'(\eta - \xi + t)\vec{\nabla} P(\eta) d\eta$$

$$\frac{\partial v}{\partial \xi} = +\int_{-\infty}^{\xi} f'(\eta - \xi + t)\vec{\nabla} P(\eta) d\eta - f(t)\vec{\nabla} P(\xi)$$

$$\frac{\partial \vec{v}}{\partial t} + \frac{\partial v}{\partial \xi} = -f(t)\vec{\nabla} P(\xi) = -\vec{\nabla}[P(\xi, t)]$$

Check

$$\vec{v}(0) = -\int_{-\infty}^{\xi} f(\eta - \xi)\vec{\nabla} P(\eta) d\eta$$

$$\eta < \xi \Rightarrow f(neg) \equiv 0$$

Inside wake: To be derived.

$$\psi = -\int_{-\infty}^{\xi} f(\eta - \xi + t) P(\eta)\, d\eta$$

Appendix II

MOMENTUM THEORY

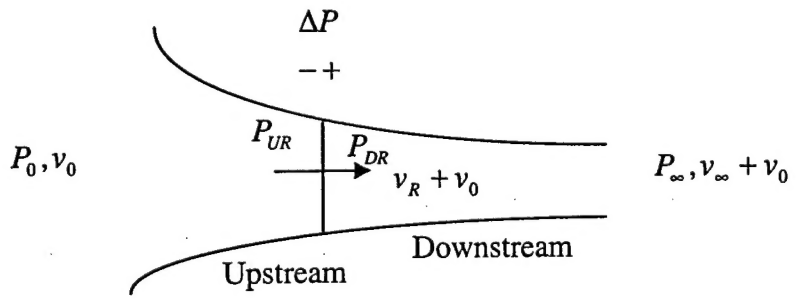

Upstream: $P_0 + \frac{1}{2}\rho v_0^2 = P_U + \frac{1}{2}\rho(v_0 + v_U)^2$

$$\boxed{P_0 - P_U = \frac{1}{2}\rho v_U (v_U + 2v_0)}$$

Downstream: $P_0 + \Delta P + \frac{1}{2}\rho v_0^2 = P_D + \frac{1}{2}\rho(v_0 + v_D)^2$

$$\boxed{P_0 - P_D + \Delta P = \frac{1}{2}\rho v_D(v_D + 2v_0)}$$

At Rotor: $P_{DR} = P_{UR} + \Delta P, \qquad v_{UR} = v_{DR} \equiv v_R$

At infinity: $\boxed{\Delta P = 2\rho v_R(v_R + v_0)}$

At Rotor:

$$P_0 - P_{UR} = \frac{1}{2}\rho v_R(v_R + v_0)$$

$$P_0 - P_{DR} + 2\rho v_R(v_R + v_0) = \frac{1}{2}\rho v_R(v_R + 2v_0)$$

$$-P_0 + P_{DR} = \frac{1}{2}\rho v_R(2v_0 + 3v_R)$$

$$\frac{P_{DR} - P_0}{P_0 - P_{UR}} = \frac{3v_R + 2v_0}{v_R + 2v_0}$$

Hover: $v_0 = 0, \quad \frac{P_{DR} - P_0}{P_0 - P_{UR}} = 3$

Low-Lift Climb $v_0 >> v$

Upstream: $P_0 - P_U = \rho v_U v_0$

Downstream: $P_0 - P_D + \Delta P = \rho v_D v_0$

At infinity: $\Delta P = 2\rho v_R v_0$

At Rotor: $\frac{P_{DR} - P_0}{P_0 - P_{UR}} = 1$

Interactions

The Principal Investigator made six trips to Boeing Helicopter Company in Mesa, Arizona, to discuss the work that is being done and how it might be integrated into their simulation codes. The presentations were also made to the Boeing Foundation in St. Louis. A trip was also made to Florida Atlantic University to discuss the inflow model with Professor Gopal Gaonkar. Three visits were made to AFTD at Ames Research Center.

Publications

1. Peters, David A. and Nelson, Adria M., "A Two-Dimensional Rotor Inflow Model Developed in Closed Form from a Galerkin Approach," Proceedings of the 18th AIAA Applied Aerodynamics Conference, Denver, Colorado, Aug. 14-17, 2000, Paper AIAA-2000-4119.
2. Peters, David A. and Nelson, Adria M., "A Dynamic Wake Model in Two Dimensions from a Galerkin Approach," AHS Aeromechanics Specialists' Meeting, Atlanta, Georgia, Nov. 13-14, 2000.
3. Peters, David A. and Morillo, Jorge A., "Towards a Complete Dynamic Wake Model in Axial Flow," AHS Aeromechanics Specialists' Meeting, Atlanta, Georgia, Nov. 13-14, 2000.
4. Peters, David A., Morillo, Jorge A., and Nelson, Adria M., "New Developments in Dynamic Wake Modeling for Dynamics Applications," Proceedings of the 57th Annual Forum of the American Helicopter Society, Washington, D.C., May 9-11, 2001.
5. Nelson, Adria M., *Inflow Equations in Two Dimensions from a Galerkin Approach,* Master of Science Thesis, Washington University in St. Louis, May 2001.
6. Morillo, Jorge A. and Peters, David A., "A Three-Dimensional Unsteady Inflow Model from a Galerkin Approach," Proceedings of the Ninth International Workshop on Aeroelasticity of Rotorcraft Systems,
7. Morillo, Jorge A., *A Fully Three-Dimensional Unsteady Rotor Inflow Model from a Galerkin Approach*, Doctor of Science Thesis, Washington University in St. Louis, December 2001.
8. Barci, Pilar Rojas, "Computation of Flow Field Above-Disk for an Activator Strip in Axial Flow," Master of Science Thesis, St. Louis University, December 2001.
9. Morillo, Jorge A. and Peters, David A., "Extension of Dynamic Inflow Models to Include Mass Injection and Off-Disk Flow," AIAA 40th Aerospace Sciences Meeting & Exhibit, Reno, Nevada, January 14-17, 2002, Paper No. AIAA 2002-0716.
10. Morillo, Jorge A. and Peters, David A., "Comparison of Exact Time-Domain Solutions for Rotor Inflow with Finite-State Results," Proceedings of the 43rd AIAA/ASME/ASCE/AHS Structures, Structural Dynamics and Materials Conference, Denver, April 22-25, 2002.
11. Rojas, Pilar, Peters, David A., and Karunamoorthy, Swami, "Two-Dimensional Inflow Above Disk for an Actuator Strip in Axial Flow," Proceedings of the 20th AIAA Applied Aerodynamics conference, St. Louis, June 24-26, 2002, AIAA Paper No. 2002-2814.
12. Morillo, Jorge A. and Peters, David A., "Convergence of a Complete Finite-State Inflow Model of a Rotor Flow Field," 28th European Rotorcraft Forum, Bristol, England, September 17-20, 2002.
13. Morillo, Jorge and Peters, David. "Velocity Field Above a Rotor Disk by a New Dynamic Inflow Model," *Journal of Aircraft*, Vol. 39, No. 5, Sept – Oct 2002.

14. Peters, David A., Morillo, Jorge A., and Nelson, Adria M., "New Developments in Dynamic Wake Modeling for Dynamics Applications," *Journal of the American Helicopter Society*, Vol. 48, No. 2, April 2003.
15. Peters, David A., "Review of Dynamic Wake Models for Application to Dynamics and Stability," Proceedings of the 4th Australian Pacific Vertiflite Conference on Helicopter Technology, Melbourne, July 21-23, 2003.
16. Yu, Ke and Peters, David A., "Use of Potential Flow State-Space Inflow Modeling for Mass Source Rotors," 29th European Rotorcraft Forum, Friedrichshafen, Germany, September 16 – 18, 2003, Paper No. 68.
17. Makinen, Stephen M. and Peters, David A., "Comparison of Prandtl and Goldstein Optimum Propeller Solutions with Dynamic Wake Models," Tenth International Workshop on Aeroelasticity of Rotorcraft Systems, Atlanta, November 3-5, 2003.
18. Yu, Ke and Peters, David A., "Net Mass Flow Components in a Three-Dimensional, Unsteady Rotor Inflow Model," ASME International Mechanical Engineering Congress and Exhibition, Washington, D.C., Nov. 17 – 21, 2003, ASME Paper IMECE2003 – 42459.
19. Yu, Michael and Peters, David A., "Three-Dimensional State-Space Modeling of Ground Effect in Dynamic Wake," 60th Annual National Forum of the American Helicopter Society, Alexandra, VA, June 7-10, 2004, pp. 100-121.
20. Yu, K. and Peters, D.A., "State-Space Inflow Modeling for Lifting Rotors with Mass-Injection," *The Aeronautical Journal*, July 2004, Paper No. 2863.

Personnel Supported

Dr. David A. Peters, PI
Michael Ke Yu, Graduate Research Assistant
Stephen Makinen, Graduate Research Assistant
Jorge Morillo, Graduate Research Assistant, D.Sc., Dec. 2001